Effect of nearest neighbor Pb-O divacancy pairs on the ferroelectric-relaxor transition in $Pb(Sc_{1/2}Nb_{1/2})O_3$

B. P. Burton and Eric Cockayne
Ceramics Division, Materials Science and Engineering Laboratory, National Institute of Standards and Technology, Gaithersburg, Maryland 20899-8520, USA

Silvia Tinte
Instituto de Desarrollo Tecnológico para la Industria Química (INTEC), Universidad Nacional del Litoral, Güemes 3450, 3000 Santa Fe, Argentina

U. V. Waghmare
J. Nehru Theoretical Sciences Unit, JNCASR, Jakkur, Bangalore 560 064, India
(Received 9 November 2007; revised manuscript received 2 March 2008; published 29 April 2008)

Molecular dynamics simulations were performed on a first-principles-based effective Hamiltonian for $Pb(Sc_{1/2}Nb_{1/2})O_3$ (PSN) with nearest neighbor Pb-O divacancy pairs. Simulations were performed for PSN with ideal chemical order, chemical short-range order, and random chemical disorder. Divacancy concentration vs temperature, $X_{[Pb\text{-}O]}$ vs T, phase diagrams were calculated, and they are shown to be topologically equivalent to the previously calculated hydrostatic pressure vs temperature diagram. In PSN with ideal chemical order, the Burns temperature defines an isotherm, which is analogous to the "Griffiths phase" in the magnetic dilution problem.

DOI: 10.1103/PhysRevB.77.144114 PACS number(s): 77.80.Bh, 61.43.−j, 61.72.Bb, 61.72.J−

I. INTRODUCTION

Perovskite-based $Pb(BB')O_3$ relaxor ferroelectrics (RFE),[1,2] such as $Pb(Sc_{1/2}Nb_{1/2})O_3$ (PSN), $Pb(Sc_{1/2}Ta_{1/2})O_3$ (PST), and $Pb(Zn_{1/3}Nb_{2/3})O_3$ (PZN), and relaxors [which have no ferroelectric (FE) ground state], such as $Pb(Mg_{1/3}Nb_{2/3})O_3$ (PMN) and $Pb(Mg_{1/3}Ta_{2/3})O_3$,[3] are technologically important transducer (actuator) materials with extraordinary dielectric and electromechanical properties. Chemically disordered PSN exhibits a RFE to normal FE transition at $T_{FE}\approx 373$ K. Chu *et al.*[4] demonstrated that the addition of 1.7 at. % Pb-O divacancies depresses the FE-transition temperature, from $T_{FE}\approx 373$ K to $T_{FE}\approx 338$ K, and broadens the temperature range in which RFE properties (e.g., frequency dispersion in the dielectric response) are observed. Chu *et al.*[4] also reported similar and more complete results for isostructural PST.[5–7] These results suggest that a sufficient concentration of divacancy pairs, $X_{[Pb\text{-}O]}$, will drive the system to a fully relaxor state without a FE ground state.

Increasing hydrostatic pressure P (Fig. 1) drives chemically disordered PSN [probably with chemical short-range order (C-SRO)] into a fully relaxor state.[8] The results of previous simulations by Tinte *et al.*[9] convincingly explained this in terms of a delicate balance between the energetics that stabilize normal ferroelectricity (proportional to FE well depths) and the spatial ensemble average strength of local random fields that promote the RFE state: (1) P has a negligible effect on the average strength of local "random fields" $\langle\vec{h}_i\rangle$ ($\langle\ \rangle$ indicates spatial averaging) that arise from the charge difference between Sc^{3+} and Nb^{5+}; (2) P smoothly and monotonically reduces FE well depths[10–12] and thus destabilizes the FE phase relative to the RFE state; (3) keeping $\langle\vec{h}_i\rangle$ approximately constant while reducing FE well depth corresponds to a *relative increase* in $\langle\vec{h}_i\rangle$. Because P does not significantly change $\langle\vec{h}_i\rangle$, it will only induce a FE⇌RFE transition, instead of a FE⇌PE transition, in a sample that has some RFE character even at $P=0$, e.g., chemically disordered PSN. In a sample without significant $\langle\vec{h}_i\rangle$, e.g., $BaTiO_3$ or $PbTiO_3$ (or PSN with perfect chemical order), moderate pressure ($P\lesssim 0.2$ GPa) induces a FE⇌PE transition.[13]

Defects such as Pb vacancies (V_{Pb}),[14] oxygen vacancies (V_O), or charge-compensating nearest neighbor (nn) Pb-O divacancy pairs ($V^{nn}_{Pb\text{-}O}$) (Ref. 15) are another source of local fields, $\langle\vec{h}_i\rangle$. Increasing $X_{[Pb\text{-}O]}$ enhances relaxor properties be-

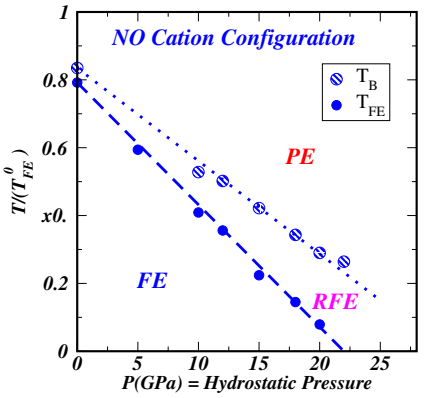

FIG. 1. (Color online) Simulated temperature vs pressure phase diagram for $Pb(Sc_{1/2}Nb_{1/2})O_3$ (Ref. 9) in the NO cation configuration: 20 chemically ordered clusters, of 800 Pb-sites each, in a percolating disordered matrix. $T^0_{FE}=T_{FE}$ in the ideally NaCl-ordered cation configuration, which has zero $V^{nn}_{Pb\text{-}O}$ divacancy. Temperature scales for all phase diagrams in this work are normalized to T^0_{FE}.

cause it *directly* increases $\langle \vec{h}_i \rangle$. In a system with sufficient chemical disorder to induce RFE characteristics at $P=0$ (e.g., chemically disordered PSN), one expects that the T vs $X_{[\text{Pb-O}]}$ phase diagram will be topologically equivalent to the T vs P phase diagram (Fig. 1). Even if $\langle \vec{h}_i \rangle = 0$ initially, e.g., as in PSN with perfect chemical order, one expects an increase in $X_{[\text{Pb-O}]}$ to induce a FE$\rightarrow$RFE transition and when $X_{[\text{Pb-O}]}$ is larger than some critical value, X_C, to induce a fully relaxor state.

In previous simulations,[16] the presence of V_{Pb} vacancies[14] or $V^{\text{nn}}_{\text{Pb-O}}$ divacancies[16] in PSN lead to more diffuse FE phase transitions with broadened dielectric susceptibility peaks; however, the RFE state was not clearly delineated. Here, simulations are used to construct $T-X_{[\text{Pb-O}]}$ phase diagrams for PSN with random, perfectly ordered and nano-ordered (NO) cation configurations; the NO configuration has 20 NaCl-type ordered clusters, per periodic supercell, in a percolating random matrix. Concentration and temperature ranges for paraelectric (PE) and FE phases, and for RFE and relaxor states, were identified from changes in polarization correlations.[9] As expected, a fully relaxor state is induced at some chemical-configuration dependent critical concentration of $V^{\text{nn}}_{\text{Pb-O}}$ divacancies, X_C, regardless of the Sc:Nb-cation configuration.

II. SIMULATIONS

Simulations were performed by using the first-principles-based effective Hamiltonian H_{eff} that is described in detail in Ref. 16; it expands the potential energy of PSN in a Taylor series about a high-symmetry perovksite reference structure, including those degrees of freedom relevant to ferroelectric phase transitions,

$$H_{\text{eff}} = H(\{\vec{\xi}_i\}) + H(e_{\alpha\beta}) + H(\{\vec{\xi}_i\}, e_{\alpha\beta}) + PV + H(\{\vec{\xi}_i\}, \{\sigma_l\}, \{V_{\text{Pb-O}}\}), \quad (1)$$

where $\{\vec{\xi}_i\}$ represents Pb-site-centered local polar distortion variables of arbitrary magnitudes and orientations, $e_{\alpha\beta}$ is the homogeneous strain term, $H(\{\vec{\xi}_i\}, e_{\alpha\beta})$ is a strain coupling term, and PV the standard pressure-volume term. The first four terms are sufficient to model pressure-dependent phase transitions in a normal FE perovskite without local fields.[17] The fifth term, $H(\{\vec{\xi}_i\}, \{\sigma_l\}, \{V_{\text{Pb-O}}\})$, represents coupling between polar variables and "random" local fields, $\vec{h}_i$,[16,18,19] from (1) screened electric fields from the quenched distribution of Sc^{3+} and Nb^{5+} ions $\{\sigma_l\}$ and (2) by V_{Pb} and V_{O}.

Experiments[20–22] on $PbTiO_3$ and $Pb(Zr_{1-X}Ti_X)O_3$ indicate distributions of V_{Pb}, V_{O}, nn Pb-O divacancy pairs, and second-nn divacancies, $V^{\text{2nn}}_{\text{Pb-O}}$, but relative proportions of the various defects were not reported, nor were concentrations of various defects. (In general, the $i$nn superscript in $V^{i\text{nn}}_{\text{Pb}}$ indicates the ith nn Pb-O divacancy pair, $i=1,2,3\ldots$, but when $i=1$, 1 is omitted and only "nn" is written). Calculations of formation energies ΔE_f for $V^{\text{nn}}_{\text{Pb-O}}$ and $V^{\text{2nn}}_{\text{Pb-O}}$ divacancies yield approximately equal values, $\approx 1.6 \pm 0.1$ eV/divacancy,[23] which suggest approximately equal populations for $V^{\text{nn}}_{\text{Pb-O}}$ and $V^{\text{2nn}}_{\text{Pb-O}}$. The simulations presented here only consider a "$V^{\text{nn}}_{\text{Pb-O}}$ approximation," in which a random distribution of nn divacancy pairs are treated as fixed $\langle 1,1,0 \rangle^{\star}$ local dipoles (superscript $\star$ indicates the "star" of 12 $\langle 1,1,0 \rangle$-type directions), i.e., this is a 12-state Potts model[24] on a subset of Pb sites. Dipole moments of the $V^{\text{nn}}_{\text{Pb-O}}$ divacancies in the $V^{\text{nn}}_{\text{Pb-O}}$ approximation are assumed to be equal to those calculated for $V^{\text{nn}}_{\text{Pb-O}}$ divacancies in $PbTiO_3$.[15] This treatment is clearly a serious simplification, but it is sufficient to elucidate qualitative trends in the FE$\rightleftharpoons$RFE transitions or temperature vs $X_{[\text{Pb-O}]}$ phase diagrams. Also, constructing a more realistic model that includes $V^{\text{nn}}_{\text{Pb-O}}$, $V^{\text{2nn}}_{\text{Pb-O}}$, $V^{\text{3nn}}_{\text{Pb-O}}$, … divacancies would require assumptions about their unmeasured relative concentrations as functions of $X_{[\text{Pb-O}]}$.

Further details of the simulations are given in the review by Burton *et al.*[16] and the study of pressure effects.[9] In all these studies, the simulation supercell contained $40\times40\times40$ unit cells, each represented by a local distortion variable at the Pb site. The same simulation cell is used here, except that $40^3 X_{[\text{Pb-O}]}$ randomly selected local distortion variables are replaced by fixed dipole moments corresponding to $V^{\text{nn}}_{\text{Pb-O}}$ divacancy pairs (i.e., local fields directed, from a Pb site, along one of the 12 $\langle 110 \rangle$-type vectors). This treatment differs from that of Bellaiche *et al.*,[14] which considered V^{2-}_{Pb} without charge-compensating V^{2+}_{O}. Presumably, the real system has charge-compensating V^{2+}_{O}, as reported by Chu *et al.*[4] The local electrical fields generated by a nn divacancy pair can be conveniently described in our model by using the point dipole approximation, while this approximation would fail for farther neighbor divacancy pairs. Nonetheless, we expect that our results are qualitatively valid for realistic vacancy distributions.

The $40\times40\times40$ simulation supercell is divided into 80 convex 800-site subregions or "clusters" of approximately equal shape. The same partition into subregions is used to investigate and contrast (1) ideal NaCl-type chemical order, where the Sc and Nb in all 80 subregions are chemically ordered (collectively and individually labeled as COR for "chemically ordered region"); (2) a random cation configuration, where the Sc and Nb in all 80 clusters are randomly chemically disordered (labeled as CDR for "chemically disordered region"); (3) a nano-ordered configuration, where 60 clusters are CDR and 20 are COR. The nano-ordered configuration is the same one that was investigated in earlier works.[9,16] It is important to study such an inhomogeneous state because of experimental observations that chemical inhomogeneity enhances relaxor properties.[25] Physically, the nano-ordered configuration has 20 distinct ordered clusters ($\sim$4 nm in diameter) in a percolating disordered matrix. Mathematically, the partition of our supercell into 80 equal regions removes size dependence from local thermodynamic averages and allows for direct comparison of the local thermodynamic averages (e.g., local polarization) between subsystems with different polar orderings and between the CDR and COR in the nano-ordered system. To analyze local polar order in the simulations, we use cluster-cluster spin products,

$$\langle \vec{S}_i(t) \cdot \vec{S}_j(t) \rangle. \quad (2)$$

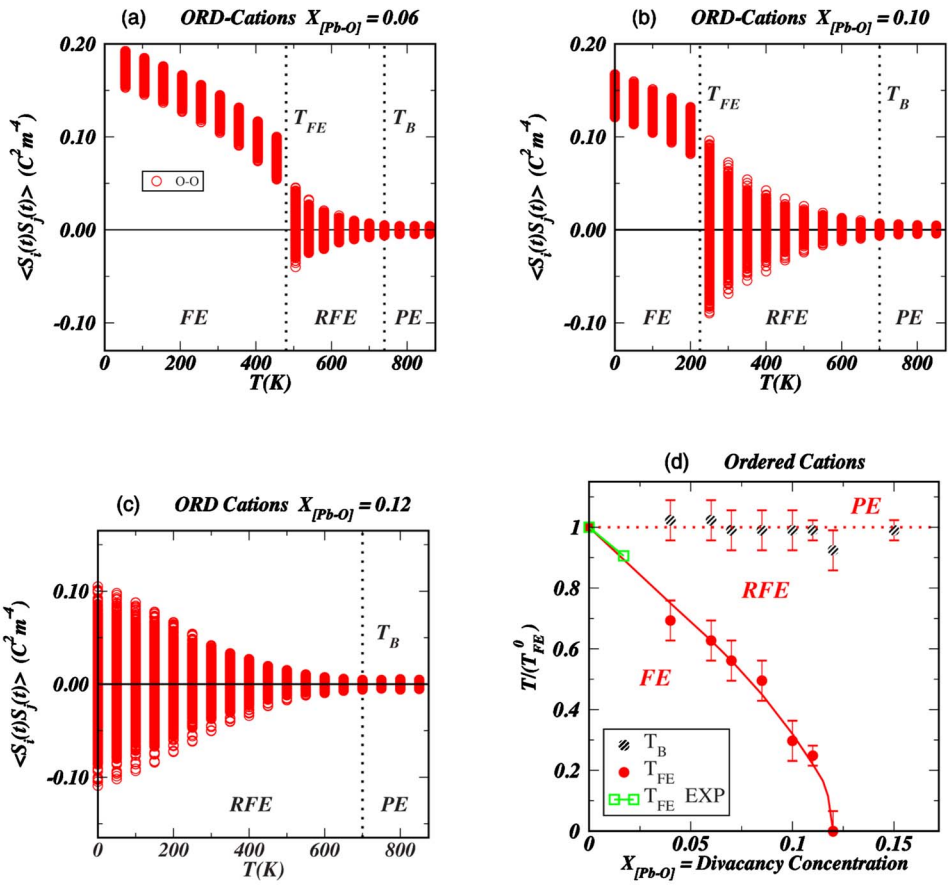

FIG. 2. (Color online) Cluster-cluster spin products, $\langle \vec{S}_i(t)\cdot\vec{S}_j(t)\rangle$, for the ideal NaCl-type chemically ordered B-site cation configuration in $Pb(Sc_{1/2}Nb_{1/2})O_3$. Increasing $X_{[Pb\text{-}O]}$ from (a) $X_{[Pb\text{-}O]}=0.06$ to (b) $X_{[Pb\text{-}O]}=0.10$ to (c) $X_{[Pb\text{-}O]}=0.12$ broadens the relaxor (RFE) field, mostly at the expense of the FE phase. (d) At a sufficiently large value, e.g., $X_C \approx 0.12$, T_{FE} disappears below 0 K and there is no FE ground state. ($T^0_{FE}=T_{FE}$ at $X_{[Pb\text{-}O]}=0$ in this ideally NaCl-ordered cation configuration). Within computational precision, and analogous to Griffiths phase behavior (Refs. 27 and 30), the Burns temperature, $T_B(X_{[Pb\text{-}O]})$, defines an isotherm that extends beyond the critical concentration of $V^{nn}_{Pb\text{-}O}$ at $X_C \approx 0.12$. Experimental data are from Chu *et al.* (Ref. 4).

The angular brackets, $\langle\ \rangle$, indicate time averaging (t) over 48 ps of molecular dynamics simulation time, while $\vec{S}_i$ and $\vec{S}_j$ are spatially averaged moments of 800-site clusters i and j. As discussed in Tinte *et al.*,[9] these spin products can be used to locate the, typically first order, PE or RFE$\rightleftharpoons$FE phase transition temperatures, T_{FE}, and approximate Burns temperatures T_B at which enhanced P-SRO and other deviations from normal PE behavior become measurable.[9,26] In the nano-ordered configuration, there are three populations of $\langle \vec{S}_i(t)\cdot\vec{S}_j(t)\rangle$: $\langle \vec{S}_i(t)\cdot\vec{S}_j(t)\rangle_{O\text{-}O}$, products between two chemically ordered clusters (COR); $\langle \vec{S}_i(t)\cdot\vec{S}_j(t)\rangle_{O\text{-}D}$, products between one COR and one chemically disordered cluster (CDR); and $\langle \vec{S}_i(t)\cdot\vec{S}_j(t)\rangle_{D\text{-}D}$, products between two CDR.

III. RESULTS

A. Ideal chemical order

Figures 2(a)–2(c) are $\langle \vec{S}_i(t)\cdot\vec{S}_j(t)\rangle$ vs $T(K)$ plots. Figure 2(d) is the simulated T/T^0_{FE} vs $X_{[Pb\text{-}O]}$ phase diagram, in which T^0_{FE} is the FE-transition temperature for a crystal with ideal chemical order and zero $V^{nn}_{Pb\text{-}O}$ divacancies at $X_{[Pb\text{-}O]}=0$. At $X_{[Pb\text{-}O]}>0$, the $V^{nn}_{Pb\text{-}O}$ divacancies are the only source of local fields, $\vec{h}_i$. The dotted line in Fig. 2(d) indicates T_B vs $X_{[Pb\text{-}O]}$ and the solid line indicates T_{FE} vs $X_{[Pb\text{-}O]}$. Clearly, increasing $\langle \vec{h}_i\rangle$ by increasing $X_{[Pb\text{-}O]}$ broadens the RFE region of the phase diagram and drives the system into a fully relaxor state at $X_C \sim 0.12$. Within the investigated range of bulk composition, $T_B(X_{[Pb\text{-}O]})$ appears to be isothermal, which suggests an analogy between the RFE state and the "Griffiths phase" (GP) in the magnetic dilution problem.[27] The apparently isothermal trend of $T_B(X_{[Pb\text{-}O]})$ is not demonstrated at high values of $X_{[Pb\text{-}O]}$, as predicted by Griffiths,[27] but clearly it extends to values of $X_{[Pb\text{-}O]}$ that are greater than $X_C \approx 0.12$.

B. Random chemical disorder

Figures 3(a) and 3(b) are plots of $\langle \vec{S}_i(t)\cdot\vec{S}_j(t)\rangle$ vs T/T^0_{FE}, and Fig. 3(c) is the $X_{[Pb\text{-}O]}$ vs T/T^0_{FE} phase diagram for the random cation configuration. Here, $T_B(X_{[Pb\text{-}O]})$ decreases, and the transitions occur at much lower temperatures than in Fig. 2, due to the combination of $\langle \vec{h}_i\rangle$ from chemical disorder

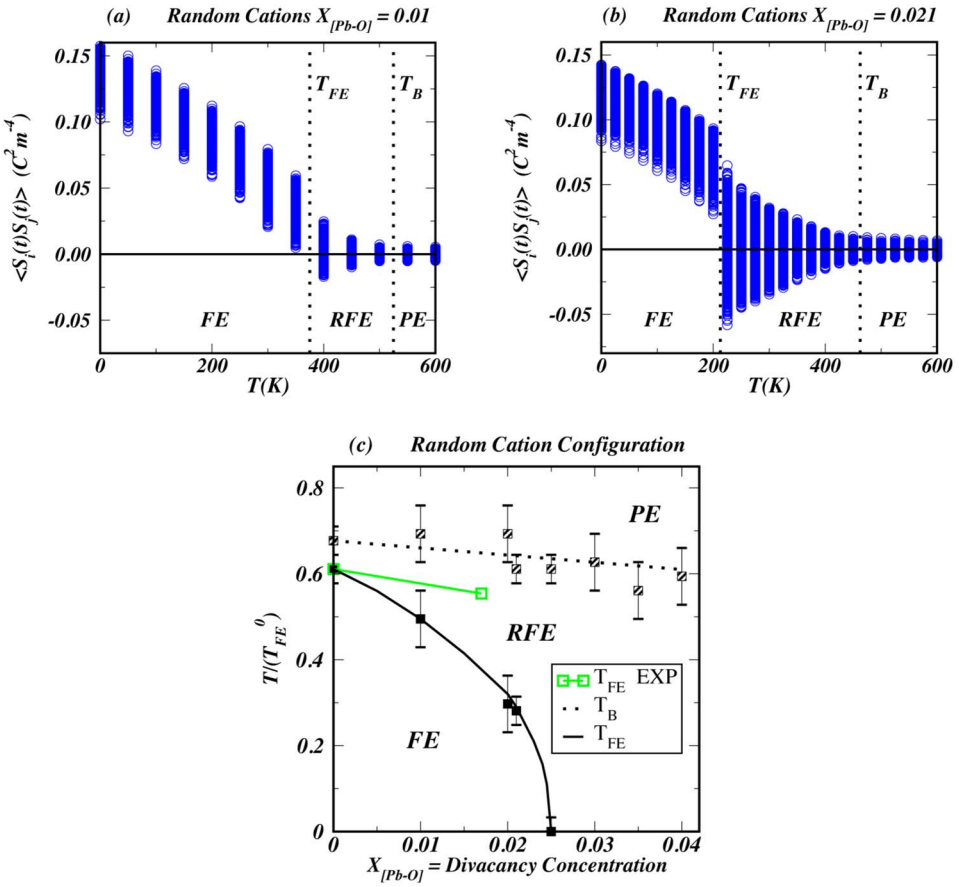

FIG. 3. (Color online) Spin products for the randomly disordered cation configuration. As for the ordered configuration, an increase in $X_{[\text{Pb-O}]}$ leads to broadening of the RFE region, and above some critical concentration, $X_C \approx 0.025$, the ferroelectric ground state is suppressed.

with $\langle \vec{h}_i \rangle$ contributions from $V^{\text{nn}}_{\text{Pb-O}}$ divacancy pairs. As in Fig. 2, $T_{\text{FE}}(X_{[\text{Pb-O}]})$ exhibits negative curvature with $X_C \approx 0.025$.

C. Nano-ordered configuration

As in Burton *et al.*,[28] the hierarchy of ensemble averages for cluster-cluster spin product magnitudes is

$$|\langle \vec{S}_i(t) \cdot \vec{S}_j(t) \rangle|_{O\text{-}O} > |\langle \vec{S}_i(t) \cdot \vec{S}_j(t) \rangle|_{O\text{-}D} > |\langle \vec{S}_i(t) \cdot \vec{S}_j(t) \rangle|_{D\text{-}D}, \tag{3}$$

reflecting the strong correlation between enhanced polar SRO and chemical SRO.[16]

In general, the temperature dependence of $\langle \vec{S}_i(t) \cdot \vec{S}_j(t) \rangle$ in the nano-ordered configuration is qualitatively similar to that in the ideally ordered and random configurations, e.g., Figs. 4(a) and 4(b): $T_B(X_{[\text{Pb-O}]})$ linearly varies and $T_{\text{FE}}(X_{[\text{Pb-O}]})$ exhibits negative curvature with $X_C \approx 0.04$. With particular distributions of $V^{\text{nn}}_{\text{Pb-O}}$ divacancy pairs [Figs. 4(c)–4(e) and 6], however, the simulation exhibited glassy freezing [(red) ● in Fig. 4(f)] rather than the expected transition to the FE phase [changing the distribution of $V^{\text{nn}}_{\text{Pb-O}}$ divacancy fields usually leads to a FE transition, often with some suggestion of freezing behavior, as in Fig. 4(e)]. In this simulation [Fig. 4(b)], the disordered matrix ($\langle \vec{S}_i(t) \cdot \vec{S}_j(t) \rangle_{D\text{-}D}$, blue dots) behaves as if the system were exhibiting fully relaxor characteristics: enhanced P-SRO below T_B but no obvious microstructure and no FE transition. The $\langle \vec{S}_i(t) \cdot \vec{S}_j(t) \rangle_{O\text{-}O}$, [Figs. 4(c) and 4(d)], however, exhibit very clear bands below a characteristic temperature, T_f (f for freezing), and T_f exhibits hysteresis: Fig. 4(c) was calculated by cooling an initially random polar distribution; Fig. 4(d) was calculated by heating an initially random polar distribution. Thus, the COR exhibit glassy freezing, while the CDR behave as though the system had fully relaxor character.

Distribution averages (*O-O*, *O-D*, and *D-D*) are indicated by solid lines in Fig. 4(a) and, as in previous simulations,[9,16,28] these exhibit positive deviations from zero at temperatures *above* T_{FE}. These deviations, which clearly bias the simulation toward a FE transition, are attributed to finite size effects; it follows that a larger system would be *more* likely to exhibit freezing not less.

Analysis of approximate average COR-polar orientations ($\sim \langle \vec{S}_i(t) \rangle$ *rounded to nearest whole numbers*, Fig 5) indicates that at 250 K, the COR fraction of system freezes into a state that is a compromise between the $\langle 1,1,1 \rangle^{\star}$ FE ground state and the fixed $\langle 1,1,0 \rangle^{\star}$ fields that represent $V^{\text{nn}}_{\text{Pb-O}}$ divacancies in the $V^{\text{nn}}_{\text{Pb-O}}$ approximation (large $\langle 1,1,0 \rangle^{\star}$ arrows, Fig. 6). Thus, the most populous states in the glassy phase at $X_{[\text{Pb-O}]}=0.025$ and $T=250$ K are

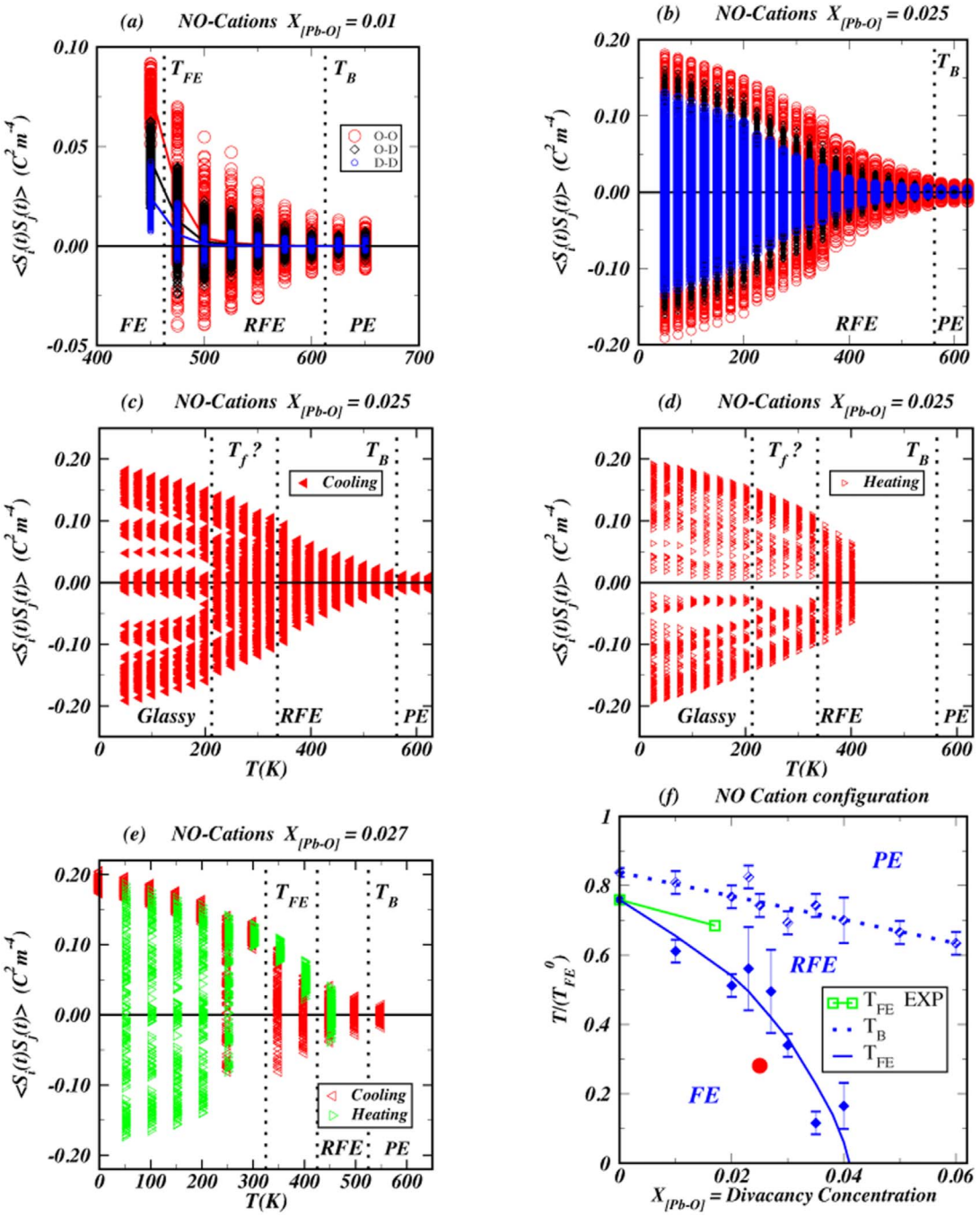

FIG. 4. (Color online) Simulation results for the nano-ordered cation configuration: (a) $\langle \vec{S}_i(t)\cdot\vec{S}_j(t)\rangle_{O\text{-}O}$, $\langle \vec{S}_i(t)\cdot\vec{S}_j(t)\rangle_{O\text{-}D}$, and $\langle \vec{S}_i(t)\cdot\vec{S}_j(t)\rangle_{D\text{-}D}$ vs T/T_{FE}^0 at $X_{[\mathrm{Pb\text{-}O}]}$=0.01; solid lines are averages for the *O-O*, *O-D*, and *D-D* distributions and their deviations from zero above T_{FE} reflect finite size effects. (b) $\langle \vec{S}_i(t)\cdot\vec{S}_j(t)\rangle_{O\text{-}O}$, $\langle \vec{S}_i(t)\cdot\vec{S}_j(t)\rangle_{O\text{-}D}$, and $\langle \vec{S}_i(t)\cdot\vec{S}_j(t)\rangle_{D\text{-}D}$ vs T/T_{FE}^0 at $X_{[\mathrm{Pb\text{-}O}]}$=0.025; the system freezes rather than transforms to the FE ground state. (c) $\langle \vec{S}_i(t)\cdot\vec{S}_j(t)\rangle_{O\text{-}O}$ vs T/T_{FE}^0 at $X_{[\mathrm{Pb\text{-}O}]}$=0.025 calculated by cooling from a random polar configuration. (d) $\langle \vec{S}_i(t)\cdot\vec{S}_j(t)\rangle_{O\text{-}O}$ vs T/T_{FE}^0 calculated on heating, from a random polar distribution. (e) $\langle \vec{S}_i(t)\cdot\vec{S}_j(t)\rangle_{O\text{-}O}$ vs T/T_{FE}^0 at $X_{[\mathrm{Pb\text{-}O}]}$=0.027; results from cooling (left-facing triangles, red) and heating (right-facing triangles, green) are superimposed, and on cooling, some tendency toward freezing is evident before transformation to the FE ground state. (f) the $X_{[\mathrm{Pb\text{-}O}]}$ vs $r\,T_{\mathrm{FE}}^0$ phase diagram; dotted line indicates $T_B(X_{[\mathrm{Pb\text{-}O}]})$, solid line indicates $T_{\mathrm{FE}}(X_{[\mathrm{Pb\text{-}O}]})$, and ● (red) at $X_{[\mathrm{Pb\text{-}O}]}$=0.025 indicates glassy freezing in cooling run (b), $X_C \approx 0.041$.

$$\langle 2,2,1\rangle = \langle 1,1,1\rangle + \langle 1,1,0\rangle \tag{4}$$

and

$$\langle 2,1,1\rangle = \langle 2,2,2\rangle - \langle 0,1,1\rangle. \tag{5}$$

In both the cooling and heating runs, only one COR occupies a $\langle 1,1,1\rangle^{\star}$ state, which is dominant in the FE ground

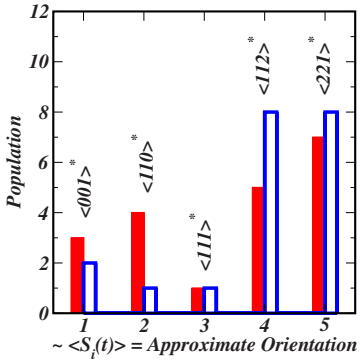

FIG. 5. (Color online) Population distributions of approximate cluster polarizations, $\sim\langle\vec{S}_i(t)\rangle$, in the 20 CORs of the frozen state at $X_{[\text{Pb-O}]}=0.25$ and $T=250$ K [(red) ● in Fig. 4(f)]. Left solid boxes (red) are from the cooling simulation [Fig. 4(c)]. Right open boxes (blue) are from the heating run [Fig. 4(d)].

state. Also, very few CORs occupy the $\langle 1,1,0\rangle^{\star}$ state that is promoted by $V^{\text{nn}}_{\text{Pb-O}}$ divacancy fields: four in the cooling run and one in the heating run. Note that $X_{[\text{Pb-O}]}=0.025$ is approximately X_C for the random system and, therefore, for the random matrix in the nano-ordered system. Thus, $X_{[\text{Pb-O}]}=0.025$ is probably the most favorable composition for glassy freezing because it combines maximal polarization in the COR with a disordered matrix that has no FE ground state.

IV. DISCUSSION

A. Phase diagrams

As suggested in the Introduction, the P vs T/T_{FE} diagram in Fig. 1 and the $X_{[\text{Pb-O}]}$ vs T/T_{FE} diagrams plotted in Figs. 2(d), 3(c), and 4(f) are topologically equivalent. Qualitatively, the only apparent difference is that in Fig. 1, $T_{\text{FE}}(P)$ is essentially linear, whereas in Figs. 2(d), 3(c), and 4(f), $T_{\text{FE}}(X_{[\text{Pb-O}]})$ exhibits some negative curvature. Note that the $T_{\text{FE}}(X_{[\text{Pb-O}]})$-transition curves in Figs. 2(d), 3(c), and 4(f) plot as lines of first-order transition rather than two-phase fields, as expected in an equilibrium diagram. Two-phase fields, separating vacancy-depleted and vacancy-enriched phases, are suppressed by the constraint that there is no vacancy diffusion during the simulations. In the real system, V_{Pb} diffusion is probably insignificant at $T\lesssim 500$ K, but V_{O} diffusion is plausible at the upper end of this range. However, immobile V_{Pb} are sufficient to suppress phase separation given that the V_{O} remain nn to the V_{Pb}.

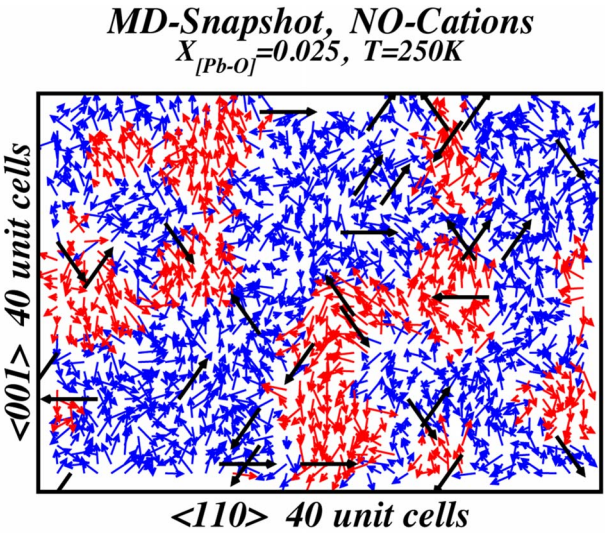

FIG. 6. (Color online) A polarization snapshot of the simulation with $X_{[\text{Pb-O}]}=0.025$, at $T=250$ K [(red) ● in Fig. 4(f)]. Each arrow represents the instantaneous polarization on a Pb-site. Ordered regions (red) have mostly homogeneous polarizations, while the random matrix (blue) exhibits more varied orientations. The $V^{\text{nn}}_{\text{Pb-O}}$ divacancy moments (black arrows) have fixed orientations along $\langle 110\rangle^{\star}$ directions, and their magnitudes are two-three times those of the most polarized Pb-atoms.

Within calculated precision, the $T_B(X_{[\text{Pb-O}]})$ curves in Figs. 2(d), 3(c), and 4(f) are linear, as in Fig. 1. Notably, $T_B(X_{[\text{Pb-O}]})$ in Fig. 2(d), for the ideal chemically ordered system, appears to be isothermal, whereas $T_B(X_{[\text{Pb-O}]})$ in Figs. 3(c) and 4(f), for the chemically random- and nano-ordered systems, exhibit negative slopes. It is not clear why $T_B(X_{[\text{Pb-O}]})$ exhibits zero slope when only $V^{\text{nn}}_{\text{Pb-O}}$ contribute to $\langle\vec{h}_i\rangle$ but a negative slope when both chemical disorder and $V^{\text{nn}}_{\text{Pb-O}}$ contribute to $\langle\vec{h}_i\rangle$. Both chemical disorder and $V^{\text{nn}}_{\text{Pb-O}}$ are treated as fixed local fields, $\vec{h}_i$, in the simulations, the only differences are that $\vec{h}_i$ from chemical disorder are much more varied in both their directions and magnitudes, while $\vec{h}_i$ from $V^{\text{nn}}_{\text{Pb-O}}$ vacancies all have identical magnitudes and only orient along $\langle 110\rangle^{\star}$-type vectors. Notwithstanding our simplified $V^{\text{nn}}_{\text{Pb-O}}$ approximation for the local fields that arise from V_{Pb}, V_{O}, $V^{i\text{nn}}_{\text{Pb-O}}$, etc., vacancies, the results presented in Figs. 2(d), 3(c), and 4(f) clearly support the interpretation that $\langle\vec{h}_i\rangle$ may be regarded as a *nonordering* field[29] that can be used to tune the proportions of RFE vs FE character in the system.

B. Relaxor–Griffiths phase analogy

In the system with ideal NaCl-type chemical order of Sc and Nb, in which $V^{\text{nn}}_{\text{Pb-O}}$ are the only source of $\vec{h}_i$, the apparently isothermal trend of $T_B(X_{[\text{Pb-O}]})$ [Fig. 2(d)] suggests that the RFE and relaxor states are analogous to the GP in the magnetic dilution problem: $[F_{1-X}N_X$ in which F is a ferromagnetic (FM) component with nn interactions, critical temperature T^0_C, and critical composition X_C and N is a nonmagnetic component[27]]. In the GP, the thermodynamic partition function of $F_{1-X}N_X$ is nonanalytic between the critical temperature of the undiluted FM system, T^0_C, and above the critical temperature of the diluted system, $T_C(X)$, hence, the isothermal trend of the transition to the GP, $T^0_C(X)=$const. Timonin[30] and Stephanovich[31] evaluated mean-field models of dilute ferroelectric systems such as $K_{1-X}Li_XTaO_3$ (KLT), which combine long-range dipole-dipole interactions with a Gaussian distribution of random fields,[30,31] and demonstrated that they exhibit GP-like singularities, hence, their predictions of the formal analogy between relaxor ferroelectrics and the GP in which T_B is analogous to $T^0_C(X)$ and $T_{\text{FE}}(X)$ is analogous to $T_C(X)$. Obviously, this analogy breaks down to some extent when the RFE⇌FE transition is first order (typically, it is weakly first order in RFE systems) or when,

as in PMN, the RFE⇌FE transition is superseded by freezing to a dipole glass. Also, the inherently long-range nature of dipole-dipole interactions in a RFE complicates the Griffiths idea of percolating magnetically ordered clusters, which are clearly defined in a magnet with nn interactions.

Note the role reversal of components in the dilute FE models relative to the magnetic dilution model:[27] in the Timonin[30] and Stephanovich[31] models, impurity doping (e.g., of off-centered Li dopants on K sites in KLT) *stabilizes* the FE-ordered phase, while the highly susceptible matrix crystal (e.g., $KTaO_3$) plays the role of the nonmagnetic N atom in the magnetic dilution problem. Hence, Fig. 1 in Stephanovich[31] has the FE phase stabilized at *high* dopant concentrations rather than at low dopant concentrations. In the PSN-based systems investigated here, $V^{nn}_{Pb\text{-}O}$ dopants are represented by *fixed* local dipole moments, which play the role of N, consistent with the magnetic dilution model.

Stephanovich[31] refers to a "…concentrational crossover between the dipole glass (electric analog of spin glass) and ferroelectricity," although his Fig. 1 indicates a phase transition between the dipole-glass and FE phases.[32] Results presented here suggest a PE⇌RFE crossover (or GP singularity[33–36]) at T_B and clearly indicate an RFE⇌FE first-order phase transition at T_{FE}. Numerical simulations are, however, inadequate to demonstrate GP nonanalyticity. Griffiths[27] argued for an isothermal onset of nonanalytic behavior throughout the compositional range ($0 \leq X < 1$ in $F_{1-X}N_X$), whereas we only investigated $X_{[Pb\text{-}O]} \leq 0.15$ because locating T_B becomes increasingly difficult as $X_{[Pb\text{-}O]}$ increases. These points merit further research, both experimental and theoretical. Note, however, that $Pb(Sc_{1/2}Ta_{1/2})O_3$, PST, is a more attractive experimental model system because it is difficult to synthesize PSN with a high degree of long-range chemical order.[37]

The analogy between RFE systems and the GP has implications for both (1) interpretation of T_B and (2) the controversy about critical exponents in RFE systems (cf. Scott[38] and Kleemann *et al.*[39]). On point (1) above, Samara[13] and Burton *et al.*[16] suggested that RFE and relaxor systems exhibit a PE⇌RFE or PE⇌relaxor crossover without a singularity at T_B, but in the magnetic systems, several studies indicate a "Griffiths singularity" at T_C^0 (cf. Imry[40] and more recent works, e.g., Refs. 33–36). Thus, if the RFE and relaxor states to GP analogy hold at T_B (analogous to T_C^0), it follows that there should be a singularity, albeit a weak singularity, rather than a crossover at T_B. On point (2) above, if the RFE⇌FE transition is analogous to the GP⇌FM transition, then the RFE⇌FE transition should exhibit GP-like exponents, at least when the system can be driven to a point of second-order transition (e.g., at appropriate pressure or applied electric field). The most plausible GP⇌FM transition analogs are the colossal magnetoresistive (CMR) systems, and experimental data on their exponents (e.g., Refs. 41 and 42 and references therein) do not support a universal set of exponents. For example, in $La_{1-X}Ca_XO_3$ with $X=0.20$ and $X=0.21$, Jiang *et al.*[42] reported $\beta=0.365$, $\gamma=1.369$, and $\delta=4.8$ and $\beta=0.09$, $\gamma=1.71$, and $\delta=20$, respectively. Unlike the RFE systems, CMR systems do not typically have the added complications of a first-order RFE⇌FE transition, or long-range interactions, and seem less likely to exhibit nonequilibrium transition-region domain formation, as emphasized by Scott.[38] Also, theory suggests that GP⇌FM exponents should vary as functions of $\langle \vec{h}_i \rangle$.[43]

C. Glassy freezing

It seems probable that the strong Potts-type character of the $V^{nn}_{Pb\text{-}O}$ approximation promotes the glassy freezing that is observed in Figs. 4(b)–4(e). A more realistic model with an equilibrium distribution of $V^{nn}_{Pb\text{-}O}$ and $V^{2nn}_{Pb\text{-}O}$, plus $V^{3nn}_{Pb\text{-}O}$, etc., divacancies, might exhibit a diminished propensity for glassy freezing. The best known experimental example of glassy freezing in a relaxor is $Pb(Mg_{1/3}Nb_{2/3})O_3$, PMN, and there is no obvious analogy between the observed chemical disorder and C-SRO and the strong Potts-type character of the $V^{nn}_{Pb\text{-}O}$ approximation. The main differences between PSN and PMN are (1) $\langle \vec{h}_i \rangle_{PMN} \approx 1.5 \langle \vec{h}_i \rangle_{PSN}$ because of the greater charge difference (Sc^{3+} and Nb^{5+} in PSN vs Mg^{2+} and Nb^{5+} in PMN)[16] and (2) the presence of strong chemical disorder induced $\langle \vec{h}_i \rangle$ in the COR of PMN, which may pin their polar moments into orientations that yield a dipole glass, as in PSN with $V^{nn}_{Pb\text{-}O}$ [Figs. 4(b)–4(d)] rather than a FE-ordered phase. There is also a clear analogy in $[K_{1-X},Li_X]TaO_3$,[44] in which off centering of Li-dopant atoms generates strong $\langle 0,0,1 \rangle^\star$, strain mediated, local fields. Thus, a system that combines significant C-SRO (as in PMN or PSN) with Li substitution should exhibit an enhanced RFE character and an enhanced propensity for glassy freezing, e.g., $[K_{0.5-X/2},Na_{0.5-X/2},Li_X]TaO_3$ with C-SRO, or clustering of Na and K, or $[Pb_{1-X},Li_X]$ $(Sc_{0.5-X/2}Nb_{0.5+X/2})O_3$.

V. CONCLUSIONS

Simulations of $PbSc_{1/2}Nb_{1/2}O_3$ with nearest neighbor Pb-O divacancies, $V^{nn}_{Pb\text{-}O}$, indicate that *directly* increasing the ensemble average local field strength $\langle \vec{h}_i \rangle$ by increasing the divacancy concentration $X_{[Pb\text{-}O]}$ enlarges the RFE state region. At $V^{nn}_{Pb\text{-}O}$ concentrations greater than the critical value, X_C, the system is in a fully relaxor state without a FE ground state. This progression mirrors nano-ordered PSN under increasing hydrostatic pressure. The essential difference is that increasing $X_{[Pb\text{-}O]}$ directly increases $\langle \vec{h}_i \rangle$, whereas increasing pressure causes a *relative* increase in $\langle \vec{h}_i \rangle$ by diminishing FE well depths while leaving $\langle \vec{h}_i \rangle$ essentially constant.

The apparently isothermal $T_B(X_{[Pb\text{-}O]})$ curve supports the prediction of Timonin[30] and Stephanovich[31] that the RFE state is analogous to the Griffiths phase in the magnetic dilution problem.[27]

Simulations of freezing, which is caused by the competition between the $\langle 1,1,1 \rangle^\star$ FE ground state, and the strong $\langle 1,1,0 \rangle^\star$ local fields, which represent $V^{nn}_{Pb\text{-}O}$ divacancies, probably do not explain glassy freezing in PMN, but they suggest a way of enhancing the propensity for glassy freezing in systems that exhibit RFE character above a FE transition, e.g., PSN.

ACKNOWLEDGMENTS

We wish to thank M. B. Weissman for suggesting that the relaxor state may be a Griffiths phase and B. E. Vugmeister for helpful discussions, particularly about the theoretical work of Stephanovich.

[1] G. A. Smolensky and A. I. Agranovskaya, Sov. Phys. Solid State **1**, 1429 (1959).
[2] L. E. Cross, Ferroelectrics **76**, 241 (1987).
[3] Here, "RFE" is used for a system, such as PSN, that exhibits a RFE⇌FE transition to a FE ground state. "Relaxor" is used for a system, such as PMN, that exhibits no FE ground state, e.g., PMN transforms to a dipole glass at $T \approx 250$ K.
[4] F. Chu, I. M. Reaney, and N. Setter, J. Appl. Phys. **77**, 1671 (1995).
[5] F. Chu, N. Setter, and A. K. Tagantsev, J. Appl. Phys. **74**, 5129 (1993).
[6] F. Chu, I. M. Reaney, and N. Setter, J. Am. Ceram. Soc. **78**, 1947 (1995).
[7] F. Chu, G. Fox, and N. Setter, J. Am. Ceram. Soc. **81**, 1577 (1998).
[8] E. L. Venturini, R. K. Grubbs, G. A. Samara, Y. Bing, and Z.-G. Ye, Phys. Rev. B **74**, 064108 (2006).
[9] S. Tinte, B. P. Burton, E. Cockayne, and U. V. Waghmare, Phys. Rev. Lett. **97**, 137601 (2006).
[10] G. Saghi-Szabo, R. E. Cohen, and H. Krakauer, Phys. Rev. Lett. **80**, 4321 (1998).
[11] M. Fornari and D. J. Singh, Phys. Rev. B **63**, 092101 (2001).
[12] R. E. Cohen, Nature (London) **358**, 136 (1992); also, R. E. Cohen and H. Krakauer, Ferroelectrics **136**, 65 (1992).
[13] G. A. Samara, Phys. Rev. Lett. **77**, 314 (1996); J. Appl. Phys. **84**, 2538 (1998); in *Fundamental Physics of Ferroelectrics 2000*, edited by R. E. Cohen (American Institute of Physics, Melville, NY, 2000), p. 344; J. Phys.: Condens. Matter **15**, R367 (2003).
[14] L. Bellaiche, J. Ìñiguez, E. Cockayne, and B. P. Burton, Phys. Rev. B **75**, 014111 (2007).
[15] E. Cockayne and B. P. Burton, Phys. Rev. B **69**, 144116 (2004).
[16] B. P. Burton, E. Cockayne, S. Tinte, and U. V. Waghmare, Phase Transitions **79**, 91 (2006).
[17] W. Zhong, D. Vanderbilt, and K. M. Rabe, Phys. Rev. Lett. **73**, 1861 (1994); K. M. Rabe and U. V. Waghmare, Phys. Rev. B **52**, 13236 (1995); U. V. Waghmare and K. M. Rabe, *ibid.* **55**, 6161 (1997).
[18] U. V. Waghmare, E. Cockayne, and B. P. Burton, Ferroelectrics **291**, 187 (2003).
[19] B. P. Burton, U. V. Waghmare, and E. Cockayne, TMS Lett. **1**, 29 (2004).
[20] D. J. Keeble, B. Nielsen, A. Krishnan, K. G. Lynn, S. Madhukar, R. Ramesh, and C. F. Young, Appl. Phys. Lett. **73**, 318 (1998).
[21] S. Gottschalk, H. Hahn, A. G. Balogh, W. Pluff, H. Kungl, and M. J. Hoffmann, J. Appl. Phys. **96**, 7464 (2004).
[22] D. J. Keeble, S. Singh, R. A. Mackie, M. Morozov, S. McGuire, and D. Damjanovic, Phys. Rev. B **76**, 144109 (2007).
[23] B. P. Burton, E. Cockayne, S. Tinte, and U. V. Waghmare, Integr. Ferroelectr. (to be published).
[24] R. B. Potts, Proc. Cambridge Philos. Soc. **48**, 106 (1952).
[25] C. A. Randall and A. S. Bhalla, Jpn. J. Appl. Phys., Part 1 **29**, 327 (1990).
[26] G. Burns and F. H. Dacol, Solid State Commun. **48**, 853 (1983).
[27] R. B. Griffiths, Phys. Rev. Lett. **23**, 17 (1969).
[28] B. P. Burton, E. Cockayne, and U. V. Waghmare, Phys. Rev. B **72**, 064113 (2005).
[29] J. M. Kosterlitz, D. R. Nelson, and M. E. Fisher, Phys. Rev. B **13**, 412 (1976).
[30] P. N. Timonin, Ferroelectrics **199**, 69 (1997).
[31] V. A. Stephanovich, Eur. Phys. J. B **18**, 17 (2000).
[32] This appears to be a different use of the term "crossover" because the boundary between a dipole-glass and a FE phase implies a change in symmetry and, therefore, a phase transition in the strict sense.
[33] R. Fisch, Phys. Rev. B **24**, 5410 (1981).
[34] A. J. Bray and M. A. Moore, J. Phys. C **15**, L765 (1982).
[35] R. R. P. Singh and S. Chakravarty, Phys. Rev. B **36**, 559 (1987).
[36] A. J. Bray, Phys. Rev. Lett. **59**, 586 (1987).
[37] C. Perrin, N. Menguy, O. Bidault, C. Y. Zahara, A. M. Zahara, C. Caranini, B. Hilczer, and A. Stepanov, J. Phys.: Condens. Matter **13**, 10231 (2001); also, N. Setter (private communication).
[38] J. F. Scott, J. Phys.: Condens. Matter **18**, 7123 (2006).
[39] W. Kleemann, J. Dec, V. V. Shvartsman, Z. Kutnjak, and T. Braun, Phys. Rev. Lett. **97**, 065702 (2006).
[40] Y. Imry, Phys. Rev. B **15**, 4448 (1977).
[41] J. Yang, Y.-P. Lee, and Y. Li, Phys. Rev. B **76**, 054442 (2007).
[42] W. Jiang, X. Zhou, G. Williams, Y. Mukovskii, and K. Glazyrin, Phys. Rev. Lett. **99**, 177203 (2007).
[43] D. Dhar, Pramana, J. Phys. **58**, 419 (2002).
[44] S. A. Prosandeev, E. Cockayne, and B. P. Burton, Phys. Rev. B **68**, 014120 (2003).